Protein Interactions

Characterizing Methyl-Bearing Side Chain Contacts and Dynamics Mediating Amyloid β Protofibril Interactions Using $^{13}C_{methyl}$-DEST and Lifetime Line Broadening**

Nicolas L. Fawzi, David S. Libich, Jinfa Ying, Vitali Tugarinov, and G. Marius Clore*

Abstract: *Many details pertaining to the formation and interactions of protein aggregates associated with neurodegenerative diseases are invisible to conventional biophysical techniques. We recently introduced ^{15}N dark-state exchange saturation transfer (DEST) and ^{15}N lifetime line-broadening to study solution backbone dynamics and position-specific binding probabilities for amyloid β (Aβ) monomers in exchange with large (2–80 MDa) protofibrillar Aβ aggregates. Here we use $^{13}C_{methyl}$ DEST and lifetime line-broadening to probe the interactions and dynamics of methyl-bearing side chains in the Aβ-protofibril-bound state. We show that all methyl groups of Aβ40 populate direct-contact bound states with a very fast effective transverse relaxation rate, indicative of side-chain-mediated direct binding to the protofibril surface. The data are consistent with position-specific enhancements of $^{13}C_{methyl}$-$R_2^{tethered}$ values in tethered states, providing further insights into the structural ensemble of the protofibril-bound state.*

The formation of protein aggregates lies at the heart of numerous degenerative diseases, including Alzheimer's disease in which the peptide amyloid β (Aβ) forms fibril plaques.[1] Because smaller aggregates of Aβ, including oligomers and protofibrils, have been implicated as the primary toxic species, they are critical targets for structural characterization.[2] Their large size, transient nature, and high level of structural disorder and heterogeneity, however, preclude characterization by standard structural techniques. Several new methods have been developed in an attempt to reveal structural details of these complexes.[3] We recently reported a new solution NMR technique, dark-state exchange

saturation transfer at backbone nitrogen positions (^{15}N-DEST), to probe, with residue-level resolution, dynamic information (^{15}N-R_2) and kinetic partitioning within the protofibril-bound state of Aβ.[4] ^{15}N-DEST and ^{15}N lifetime line-broadening exploit the binding/unbinding of monomeric Aβ peptides to/from large protofibrillar aggregates and the vastly different transverse relaxation rates (^{15}N-R_2) between monomers and protofibril-bound species to imprint atomic resolution information for the NMR-invisible ("dark") protofibril-bound state onto the easily observed resonances of the free monomer. Unlike Aβ fibrils that are stabilized by β-sheets spanning ten residues in length in both the central and C-terminal hydrophobic regions,[5] transient contacts with Aβ protofibrils are concentrated only in stretches of four to five hydrophobic residues. Since ^{15}N-DEST reports only on the backbone, ^{13}C-based experiments are required to probe side-chain contacts within the protofibril-bound states and to ascertain whether the transient interactions on the surface of the protofibrils are directly mediated by side chains or involve edge-on β-sheet contacts with effectively disordered side chains. Here we use $^{13}C_{methyl}$ DEST and lifetime broadening to refine the atomic-level picture of the interactions between monomeric and protofibrillar Aβ40. We show that methyl groups in hydrophobic side chains directly mediate interactions on the protofibril surface and are sensitive reporters of dynamics in the bound-state ensemble.

U-[$^{13}C/^{15}N$]-labeled Aβ40 (rPeptide, Bogart, Georgia, USA) was prepared from NaOH treated stocks as described previously to remove preformed aggregates and seeds.[4,6] NMR samples of 50 and 240 μM U-[$^{13}C/^{15}N$] Aβ40 were prepared in 50 mM HEPES buffer, pH 6.8 in 90% H_2O/10% D_2O from solutions stirred and filtered with Chelex 100 (Sigma) to remove trace metals. Samples were kept at 4 to 10°C and all experiments were conducted at 10°C. Assignment of the resolved methyl groups of monomeric Aβ40 was achieved using standard 3D heteronuclear correlation experiments (see the Supporting Information (SI), Figure S1) to correlate ^1H and ^{13}C methyl resonances with the previously assigned backbone $^1H_N/^{15}N$ and $^1H_\alpha/^{13}C_\alpha$ resonances.[4,7] Under these conditions, unstirred samples containing 240 μM Aβ40 spontaneously form large (2–80 MDa) polymorphic protofibrils, whereas dilute control (50 μM) samples remain > 95% monomeric.[4] After one week equilibration of the unstirred 240 μM Aβ40 sample, approximately 100 μM Aβ40 remains monomeric, whereas the balance of the peptide is sequestered in the protofibrillar aggregates visible by transmission electron and atomic force microscopy, and observed by analytical ultracentrifugation and dynamic light scattering.[4] After the initial week-long period of protofibril

[*] Dr. N. L. Fawzi
Department of Molecular Pharmacology
Physiology and Biotechnology, Brown University
Providence, RI 02912 (USA)
E-mail: nicolas_fawzi@brown.edu

Dr. D. S. Libich, Dr. J. Ying, Dr. V. Tugarinov, Dr. G. M. Clore
National Institute of Diabetes and Digestive and Kidney Diseases
National Institutes of Health
Bethesda, MD 20892-0520 (USA)
E-mail: mariusc@mail.nih.gov

assembly, the monomeric population remains in pseudo-equilibrium with the protofibril form for about one month, during which time the monomeric peptide reversibly binds to and unbinds from the protofibrils, resulting in near-zero net further assembly.[4]

The protofibril-bound species exchanging with the remaining monomeric pool is invisible to standard solution NMR methods, because it is sparsely populated ($\approx 5\%$ of the remaining monomer) and characterized by very rapid transverse relaxation rates (^{15}N-R_2 up to ca. 19000 s^{-1}) due to its very large size.[4] Interactions, however, between monomeric and protofibrillar Aβ are evident by measuring backbone-lifetime-broadening effects (ΔR_2), independent of field and nucleus, from the difference in ^{15}N-R_2 or ^{1}H$_N$-R_2 values in the presence (high concentration) and absence (low-concentration control) of protofibrils.[6b] The apparent first-order association rate constant (k_{on}^{app} for monomer-binding to the protofibril, given by the maximum value of ^{15}N-ΔR_2,[6b] is 2.5 ± 0.3 s^{-1} for U-[^{13}C/^{15}N] Aβ40 at 240 μm (SI, Figure S2).

To compare the values measured at the backbone to those measured at the side-chain methyl positions, effective ^{13}C$_{methyl}$-R_2 values were determined from ^{13}C-$R_{1\rho}$ (1666 Hz spin-lock field-centered at 20.7 ppm) and ^{13}C-R_1 values using standard experiments and procedures (SI, Figures S3 and S4).[8,9] ^{13}C$_{methyl}$ lifetime line-broadening, (^{13}C$_{methyl}$-ΔR_2), given by the difference in ^{13}C$_{methyl}$-R_2 values between Aβ40 samples in the presence and absence of protofibril aggregates (Figure 1 A), shows a position-specific pattern of interactions with the protofibrils. ^{13}C$_{methyl}$-DEST measurements confirm the residue-specific nature of the interactions (Figure 1 B). Briefly, the ^{13}C$_{methyl}$-DEST pulse sequence (SI, Figure S5) resembles a 2D ^{1}H-^{13}C HSQC-based ^{13}C-R_1 experiment, in which ^{13}C$_z$ polarization is prepared; however, the variable delay used to measure R_1 is replaced by a fixed 480 ms ^{13}C saturation pulse (radiofrequency field strengths of 763 and 1523 Hz) applied at a series of offsets from the ^{13}C carrier frequency at 19 ppm ($-23.7, -20, -16, -10 -8, -6, -4, -2, 0, 2, 4, 6, 8, 10, 16, 20, 23.7$ 26 kHz). Whereas the ^{13}C$_{methyl}$-DEST pulse sequence is similar to the recently described ^{13}C$_{methyl}$-CEST experiment,[10] the DEST and CEST experiments are not the same and should not be confused with one another: CEST relies on differences in chemical shifts between slowly exchanging species with the same or approximately the same R_2 rates, whereas DEST is entirely reliant on the exchange between species with very large differences in R_2 rates and requires no differences in chemical shifts. Further, distinct chemical shifts for the minor species will not be observed in a CEST experiment when the R_2 values for the minor species are very large. Thus, the experimental considerations for and quantitative analysis of the DEST and CEST experiments are quite different.

The data from ^{13}C$_{methyl}$ ΔR_2 and DEST experiments were fit simultaneously to the same kinetic model previously used for the corresponding ^{15}N data[4] to provide atomic-resolution details on the role of methyl-side-chain interactions in protofibril-bound states. Our previous ^{15}N data, which probed the backbone of Aβ, showed that the ensemble of binding modes in the protofibril-bound state could not be described by a simple global two-state exchange model.[4] The
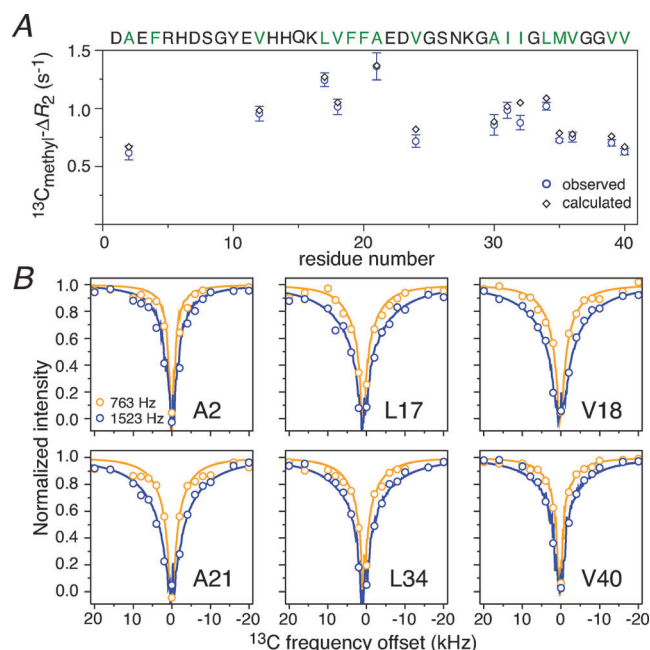

Figure 1. ^{13}C$_{methyl}$ ΔR_2 and DEST data for Aβ40. A) Observed ^{13}C$_{methyl}$-ΔR_2 (blue circles), the difference in effective R_2 of methyl group ^{13}C spins in the presence (240 μm total Aβ) and absence (50 μm Aβ) of protofibrils, are well-matched by values calculated from best-fits to the equilibrium direct-contact/tethered state binding model (black diamonds; cf. Figure 2). Values for residues (Val and Leu) with two methyl groups are averaged. Error bars are 1 s.d. The amino acid sequence is displayed on top with hydrophobic residues colored in green. B) Examples of experimental (open circles) and best-fit (solid lines) ^{13}C$_{methyl}$-DEST profiles at two radiofrequency field strengths, 763 (orange) and 1523 (blue) Hz, for methyl groups of alanine (A2 and A21), leucine (L17 and L34), and valine (V18 and V40). The best-fits obtained by nonlinear minimization and numerical integration of the McConnell equations for the direct-contact/tethered state model[4] (cf. Figure 2) by optimization of a single global ^{13}C$_{methyl}$-$R_2^{contact}$ value and residue-specific ^{13}C$_{methyl}$-$R_2^{tethered}$ values and partition coefficients (K_3) between direct-contact and tethered states, with the global pseudo-first order association rate constant k_{on}^{app} set to ^{15}N-ΔR_2^{max} (2.5 s^{-1}; SI Figure S2), and the global dissociation rate constant k_{off} (51 s^{-1}) taken from Ref. [4]. The experimental data were recorded at a spectrometer ^{1}H frequency of 600 MHz.

same is true for the current ^{13}C$_{methyl}$ data, for which the simple two-state exchange model predicts ^{13}C$_{methyl}$ ΔR_2 values and DEST profiles that are larger and narrower, respectively, than measured. However, a simple extension, incorporating slowly interconverting exchange between distinct bound states for each residue, described by a residue-specific partition coefficient K_3 for the population ratio of direct-contact to tethered states (Figure 2), is sufficient to reproduce the ^{15}N-DEST and ^{15}N-ΔR_2 data.[4] This phenomenological extension of a two-state exchange model concisely captures the average behavior of the potentially very large ensemble of bound conformations using only two distinct residue-specific parameters, the partition coefficients K_3 and the $R_2^{tethered}$ values for the tethered states. Here, we show that without expanding the model, we capture the ^{13}C$_{methyl}$ experimental data by constraining the global values of k_{on}^{app} to the value of ^{15}N-ΔR_2^{max} measured on the 240 μm ^{13}C/^{15}N-labeled Aβ40 sample (SI,
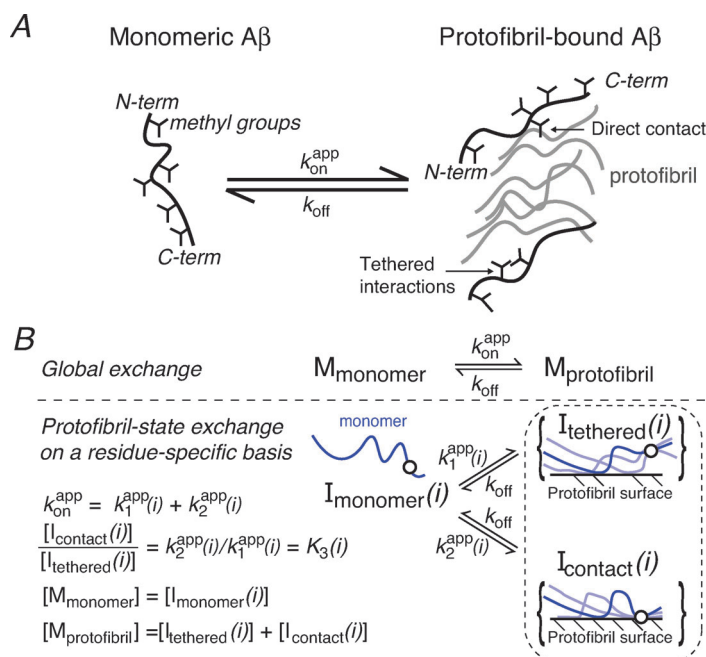
Figure 2. Interaction of monomeric Aβ on the surface of Aβ protofibrils. A) Schematic of overall exchange process. B) The direct-contact/tethered bound-state model, which incorporates tethered and direct-contact states for each residue when bound to the protofibril surface, superimposed on a global two-state exchange model.

Figure 3. Best-fit values of A) the partition coefficients K_3 (blue) and B) $^{13}C_{methyl}$-$R_2^{tethered}$ (blue). Values for the corresponding K_3 values obtained previously from ^{15}N data[4] (black) and experimental values of $^{13}C_{methyl}$-$R_2^{monomer}$ for the monomeric state (black) are also shown in panels (A) and (B), respectively. Values for residues (Val and Leu) with two methyl groups are averaged. For reference, $^{13}C_{methyl}$-$R_2^{contact}$, the best-fit value of the transverse relaxation rate, common to all methyl groups when in direct contact with the protofibril surface, is $1330\pm80\ s^{-1}$. Error bars are 1 s.d. The amino acid sequence is displayed on top with hydrophobic residues colored in green.

that k_{off} is consistent with a range of values from about 20 to 200 s^{-1} with statistically equivalent fits vis-à-vis residuals; hence we chose to fix k_{off} to the same value as determined previously,[4] which should be independent of the Aβ40 concentration and facilitate the comparison between the current results and our previous work.)

A comparison of the experimental and computed ^{13}C-methyl ΔR_2 (Figure 1 A) and $^{13}C_{methyl}$-DEST profiles (Figure 1 B) for the best-fit solution demonstrates that the model in Figure 2 B describes the ensemble of interactions well. The ability to quantitatively match the observed $^{13}C_{methyl}$-DEST profiles and $^{13}C_{methyl}$-ΔR_2 values (Figure 1) with K_3 partition coefficients similar to those determined for the backbone (Figure 3 A) demonstrates the ability of the model to capture the essential interactions present in transient monomer–protofibril binding. The high correlation between the population of direct contact states (i.e. K_3) obtained from the $^{13}C_{methyl}$ and ^{15}N data for all residues (Fig-

Figure S2), and k_{off} to that determined previously,[4] and varying the residue-specific $^{13}C_{methyl}$-$R_2^{tethered}$ relaxation rates and partition coefficients K_3, as well as a single global value of the transverse relaxation rate ($^{13}C_{methyl}$-$R_2^{contact}$) when a methyl group is in direct contact with the protofibril surface. (Note
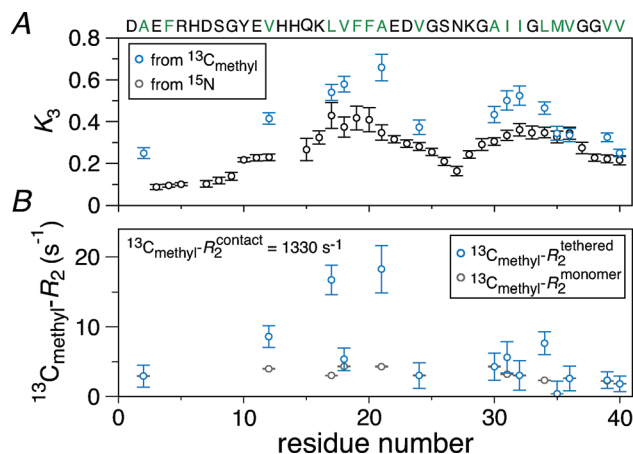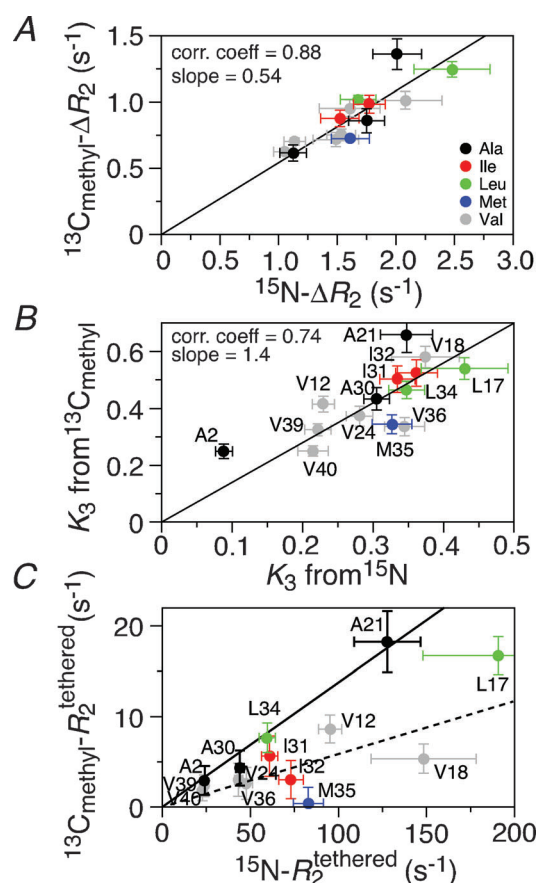

Figure 4. Correlation between A) experimental side-chain $^{13}C_{methyl}$-ΔR_2 and backbone ^{15}N-ΔR_2 values, B) best-fit direct contact/tethered partition coefficients K_3 obtained from $^{13}C_{methyl}$ and backbone ^{15}N data; and C) best-fit $^{13}C_{methyl}$-$R_2^{tethered}$ and ^{15}N-$R_2^{tethered}$ values for Aβ40. Values for residues (Val and Leu) with two methyl groups are averaged. Color coding: black, Ala; red, Ile ($C_{\gamma methyl}$); green, Leu; blue, Met; and grey, Val. ^{15}N values could not be determined for Ala2 owing to water exchange and are represented here by values for Glu3. Error bars are 1 s.d.

ure 4B), including the long, highly flexible methionine side chain, indicates that the entire side chain plays a role in mediating direct contacts with the protofibrils. The values of K_3 determined from the $^{13}C_{methyl}$ data are systematically larger than those from the ^{15}N data. Whether this truly reflects a different partitioning of bound and tethered states as viewed by the methyl groups, or whether these differences, which are less than a factor of 2 in an equilibrium constant, simply reflect sample variation, cannot be ascertained, because almost equally good fits to the data can be obtained using the K_3 values determined previously from the ^{15}N data[4] (SI, Figure S6), further emphasizing the role of the side chains in mediating direct contacts at the protofibril surface.

The global best-fit value of $^{13}C_{methyl}$-$R_2^{contact}$ (at a ^1H frequency of 600 MHz) is $1330 \pm 80\,s^{-1}$. This value, which corresponds to a homogenous line width of 3 ppm, is consistent with direct methyl group interactions with the surface of large (2–80 MDa) protofibril aggregates. Importantly, these direct interactions, though less frequent, are present even for residues such as Ala2 (Figure 1B), in the hydrophilic N-terminal region of Aβ.

The most important additional observations enabled by the $^{13}C_{methyl}$ ΔR_2 and DEST experiments relate to the behavior of the side chains in the tethered states. Our previous ^{15}N results suggested that the backbone R_2 in the tethered state varies as the average number of residues between the direct contact residue(s) and the residue of interest varies, with the highest ^{15}N-$R_2^{tethered}$ values (shortest tether) for residues 17–20. However, the role of side-chain atoms in tethered states could not be ascertained, and the relative contribution of a single side chain is obscured, because backbone motions are highly correlated along the peptide chain.[4]

The good correlation between the experimental backbone ^{15}N-ΔR_2 and side chain $^{13}C_{methyl}$-ΔR_2 values (correlation coefficient of 0.88) demonstrates the consistency between lifetime line-broadening at backbone and side-chain positions (Figure 4A). However, the $^{13}C_{methyl}$-ΔR_2 values are about half of those of the ^{15}N-ΔR_2 values, as expected since $^{13}C_{methyl}$-$R_2^{contact}$ is only about 20-fold higher than k_{off}, such that $^{13}C_{methyl}$-R_2^{max} does not reach the limiting value of k_{on}^{app}.

The validity of the model used to analyze the ^{13}C-methyl data is further evidenced by the high degree of correlation between $R_2^{tethered}$ values for side-chain methyl groups and the ^{15}N backbone of alanine residues (correlation coefficient = 0.99). The effective values of $^{13}C_{methyl}$-$R_2^{tethered}$ (Figure 3B, blue circles) for the three alanine residues, whose methyl groups at Cβ reflect the backbone motion, are much higher for Ala21 compared to Ala30 and Ala2 (Figure 3B), just as those at the corresponding ^{15}N positions (Figure 4C, black circles, and solid black line).

The deviation of other methyl-bearing residues from the linear correlation between alanine $^{13}C_{methyl}$ and ^{15}N $R_2^{tethered}$ values (Figure 4C, solid line) shows the ability of the ^{13}C-methyl experiments to provide additional information regarding the motion of particular side chains in the tethered state. Some residues, such as Leu34 and Val39, fall along the same correlation line as the alanine residues, indicating that their side chains behave much like the backbone. The remaining residues, however, fall below the alanine correlation with

correspondingly smaller, but still well correlated, $^{13}C_{methyl}$-$R_2^{tethered}$ values relative to the ^{15}N-$R_2^{tethered}$ values (Figure 4C, dashed line with correlation coefficient of 0.85 and a slope value half of that for the alanine correlation) suggesting that the average distance of these methyl groups to the nearest direct contact point is further away than for the backbone.

Within the central hydrophobic region, the values of $^{13}C_{methyl}$-$R_2^{tethered}$ for Leu17 and Ala21 are high, consistent with our previous observations for the corresponding backbone ^{15}N-$R_2^{tethered}$ values.[4] A lower than expected $^{13}C_{methyl}$-$R_2^{tethered}$ value, however, is observed for Val18 compared to the adjacent Leu17 despite one fewer dihedral angle degree of freedom separating the methyl groups from the backbone, suggesting exclusion of Val18 from transient-tethered-state interactions. Conversely, although the ^{15}N-$R_2^{tethered}$ values for Val18 are 50% higher than those for Val12, the $^{13}C_{methyl}$-$R_2^{tethered}$ value for Val18 is about 30% lower, suggesting a greater degree of involvement of the Val12 side chain in transient intermolecular contacts in the tethered states than discernable from ^{15}N-DEST alone. Finally, the value of $^{13}C_{methyl}$-$R_2^{tethered}$ for Met35 is significantly lower than that for neighboring residues, indicating that its long side chain retains considerable mobility when not directly in contact with the protofibril surface. (It should be noted that one would not expect to directly observe methyl cross-peaks for the tethered states, even in cases, in which the $^{13}C_{methyl}$-$R_2^{tethered}$ values are low, as at the C-terminus, because the tethered state may be identical in chemical shift to the monomer state, and more importantly any potential cross-peak for a tethered state would be highly broadened in both ^1H and ^{13}C dimensions by the off-rate of $51\,s^{-1}$ due to the highly skewed populations of free and bound Aβ40 exchanging on the surface of the protofibrils.)

The fits reported for the $^{13}C_{methyl}$ DEST and ΔR_2 data in Figures 1, 3, and 4 were obtained with optimized values of K_3. However, as noted above, almost equally good fits can be obtained by constraining the values of K_3 to those obtained previously from analysis of the ^{15}N data.[4] The $^{13}C_{methyl}$-$R_2^{tethered}$ values obtained in this manner are highly correlated to those obtained with optimized K_3 values (SI, Figure S6) and hence do not impact the conclusions drawn above. The absolute values of $^{13}C_{methyl}$-$R_2^{tethered}$ as well as the value of $^{13}C_{methyl}$-$R_2^{contact}$, are about 60–70% higher when K_3 is fixed. This is simply due to the fact that the values of K_3 and $^{13}C_{methyl}$-R_2 in the bound state are partially anticorrelated such that higher values of K_3 (when optimized) lead to lower values of $^{13}C_{methyl}$-R_2 in the bound state.

Our current $^{13}C_{methyl}$ data support a model in which protofibril-bound structures are stabilized by a network of residues (based on the consistency of ^{15}N and $^{13}C_{methyl}$ DEST profiles), whereas methyl-bearing residues contribute to substructures in the tethered states. Further, the current work confirms the validity of the "model-free" representation of the very large ensemble of states that can be sampled on the surface of the protofibrils (Figure 2).

In summary, our analysis combining $^{13}C_{methyl}$ DEST and ΔR_2 measurements brings a new, detailed view of the structural and dynamic properties of side-chain methyl groups in exchanging systems involving very high molecular

weight (>1 MDa), transient complexes, and provides direct insight into interactions in the vicinity of a given methyl side chain that are inaccessible by other methods. Moreover, the rapid rotation of methyl groups resulting in a large reduction of $R_2^{contact}$ relative to the backbone, should permit $^{13}C_{methyl}$ DEST and lifetime line-broadening to be applied to a much larger variety of systems involving both larger NMR-observed species (e.g. greater than 100 kDa) for which the observation of backbone amides would not be feasible, larger dark states (in excess of 80 MDa), and faster exchange kinetics down to the millisecond time scale. Further extension of DEST to all nonmethyl ^{13}C atoms is also possible, but lower signal-to-noise and significant overlap precluded the complete characterization of other side-chain positions in Aβ40.

[1] J. Hardy, D. J. Selkoe, *Science* **2002**, *297*, 353–356.
[2] D. M. Walsh, D. J. Selkoe, *J. Neurochem.* **2007**, *101*, 1172–1184.
[3] a) R. Riek, P. Guntert, H. Dobeli, B. Wipf, K. Wuthrich, *Eur. J. Biochem.* **2001**, *268*, 5930–5936; b) S. Narayanan, B. Reif, *Biochemistry* **2005**, *44*, 1444–1452; c) N. Carulla, M. Zhou, M. Arimon, M. Gairi, E. Giralt, C. V. Robinson, C. M. Dobson, *Proc. Natl. Acad. Sci. USA* **2009**, *106*, 7828–7833; d) M. Ahmed, J. Davis, D. Aucoin, T. Sato, S. Ahuja, S. Aimoto, J. I. Elliott, W. E. Van Nostrand, S. O. Smith, *Nat. Struct. Mol. Biol.* **2010**, *17*, 561–567; e) H. A. Scheidt, I. Morgado, S. Rothemund, D. Huster, M. Fandrich, *Angew. Chem.* **2011**, *123*, 2889–2892; *Angew. Chem. Int. Ed.* **2011**, *50*, 2837–2840; f) H. A. Scheidt, I. Morgado, D. Huster, *J. Biol. Chem.* **2012**, *287*, 22822–22826; g) A. R. Ladiwala, J. Litt, R. S. Kane, D. S. Aucoin, S. O. Smith, S. Ranjan, J. Davis, W. E. Van Nostrand, P. M. Tessier, *J. Biol. Chem.* **2012**, *287*, 24765–24773; h) I. Bertini, G. Gallo, M. Korsak, C. Luchinat, J. Mao, E. Ravera, *ChemBioChem* **2013**, *14*, 1891–1897.
[4] N. L. Fawzi, J. Ying, R. Ghirlando, D. A. Torchia, G. M. Clore, *Nature* **2011**, *480*, 268–272.
[5] J. X. Lu, W. Qiang, W. M. Yau, C. D. Schwieters, S. C. Meredith, R. Tycko, *Cell* **2013**, *154*, 1257–1268.
[6] a) L. Hou, H. Shao, Y. Zhang, H. Li, N. K. Menon, E. B. Neuhaus, J. M. Brewer, I. J. Byeon, D. G. Ray, M. P. Vitek, T. Iwashita, R. A. Makula, A. B. Przybyla, M. G. Zagorski, *J. Am. Chem. Soc.* **2004**, *126*, 1992–2005; b) N. L. Fawzi, J. Ying, D. A. Torchia, G. M. Clore, *J. Am. Chem. Soc.* **2010**, *132*, 9948–9951; c) A. E. Conicella, N. L. Fawzi, *Biochemistry* **2014**, *53*, 3095–3105.
[7] T. Yamaguchi, K. Matsuzaki, M. Hoshino, *FEBS Lett.* **2011**, *585*, 1097–1102.
[8] D. S. Libich, N. L. Fawzi, J. Ying, G. M. Clore, *Proc. Natl. Acad. Sci. USA* **2013**, *110*, 11361–11366.
[9] L. E. Kay, T. E. Bull, L. K. Nicholson, C. Griesinger, H. Schwalbe, A. Bax, D. A. Torchia, *J. Magn. Reson.* **1992**, *100*, 538–558.
[10] a) P. Vallurupalli, G. Bouvignies, L. E. Kay, *J. Am. Chem. Soc.* **2012**, *134*, 8148–8161; b) G. Bouvignies, L. E. Kay, *J. Biomol. NMR* **2012**, *53*, 303–310; c) A. L. Hansen, G. Bouvignies, L. E. Kay, *J. Biomol. NMR* **2013**, *55*, 279–289; d) P. Vallurupalli, G. Bouvignies, L. E. Kay, *ChemBioChem* **2013**, *14*, 1709–1713; e) G. Bouvignies, P. Vallurupalli, L. E. Kay, *J. Mol. Biol.* **2014**, *426*, 763–774.